RC Coupling Beams with Different Numbers of Transverse Reinforcements Tested under Seismic or Wind Loads

Tse-An CHOU[1], Seung Heon LEE[2] and Thomas H.-K. KANG[3]

SUMMARY

In high-rise buildings, reinforced concrete (RC) coupling beams play an important role in doors and windows opening, lateral force resistance, and energy dissipation for wall systems. It is well known that diagonally RC coupling beams (DRCCBs) have superiority in shear strength, ductility, and energy dissipation over longitudinally RC coupling beams (LRCCBs). With the goal of examining the modeling parameters for RC coupled wall systems utilized in moderate-to-high seismicity and/or high wind speed areas, DRCCBs with 67% and 50% of the ACI 318 requirement for transverse reinforcement are compared to LRCCBs with 100% and 67% of the requirement in this study. Two RC coupling beams of each specimen type were tested under simulated seismic and wind events, respectively. In this study, through the application of a wind load reduction factor (R_{WR}) of 1.4, the experiment results subjected to the wind load can be deemed as a verifying example of the structural element test for performance-based wind design.

Keywords*: RC coupling beam; seismic load; wind load; performance-based design.*

INTRODUCTION

Buildings are getting taller and taller in this era due to a rapidly expanding population. Reinforced concrete (RC) coupling beams are typically designed with a span-depth ratio (l_n/h) of 2.4 for residential use and 3.3 for office use in high-rise buildings (Naish et al. 2013) due to their benefits of providing openings and forming an effective energy-dissipating system for resisting lateral loads. According to ACI 318-19 design procedure, RC coupling beams with a span-depth ratio between two and four can be configured either as a longitudinally RC coupling beam (LRCCB) or a diagonally RC coupling beam (DRCCB). Among them, DRCCBs exhibit superior capacities of shear strength, deformation, and energy dissipation than LRCCBs, due to their well-rounded hysteretic loops without pinching effect. However, many experimental outcomes of DRCCBs showed notably larger values of peak shear strength than the nominal shear strength and upper limit in ACI 318-19 (Naish et al. 2013; Lim et al. 2016a and 2016b; and Cheng et al. 2019). These two formulas may need to be modified for preventing over-conservative design that may result in insufficiently developing plastic hinges in DRCCBs which lead to undesirable forces or damage in adjacent walls (Lim et al. 2016b). Furthermore, since the number of transverse reinforcements can significantly affect the cyclic behavior and failure mode of a DRCCB (Han et al. 2019), LRCCBs and DRCCBs with fewer numbers of transverse reinforcements were investigated in this study for assessing the feasibility of usage in low-to-moderate seismicity and/or high wind speed areas.

For high-rise buildings, certain structural elements including coupling beams are typically dictated by wind requirements (Aswegan et al. 2017). The latest ASCE 7-22 (2022) provision now permits performance-based wind design with inelastic response under 700-to-3000-year mean recurrence interval (MRI) wind loads in ASCE (2019). Among components of wind load, the response of across-wind is generally larger than along-wind

[1] *Ph.D. Student, Dept. of Architecture and Architectural Engineering, Seoul National University, Seoul National University, Korea.*
[2] *Ph.D. Student, Dept. of Architecture and Architectural Engineering, Seoul National University, Seoul National University, Korea.*
[3] *Professor, Dept. of Architecture and Architectural Engineering, Seoul National University, Seoul National University, Korea; E-mail: tkang@snu.ac.kr*

due to its large resonant response (Alinejad et al. 2020), and using wind load reduction factors (R_{WR}) to reduce the design wind force (resonant component only) could significantly decrease the design demand of a coupling beam and also increase the ductility of the system (Jeong et al. 2021). While Abdullah et al. (2020) tested RC coupling beams under a 3000 MRI wind load and only minor cracks were observed in their final states, the inelastic responses of LRCCBs and DRCCBs with different numbers of transverse reinforcements subjected to the simulated wind load were investigated in this study.

EXPERIMENTAL PROGRAM

Test specimens

In this study, four layouts including L100, L67, D67 and D50 series were tested by applying seismic (named "Series-S") and wind loads (named "Series-W"). Eight two-thirds-scale RC coupling beams with a span-depth ratio (clear length/depth, l_n/h) of 2.5 were designed based on typical RC coupling beams seen in residential buildings. The cross-sectional dimensions (width × depth × span, $b_w \times h \times l_n$) of specimens were 300 mm × 500 mm × 1250 mm (11.8 in. × 19.7 in. × 49.2 in). All details, with the exception of the reduction of transverse reinforcements for study purposes, were designed in accordance with the design procedure specified in ACI 318-19. Transverse reinforcements were reduced to 67% for L67 and D67 series, and 50% for D50 series. The illustration of specimen layouts is shown in **Figure 1**.

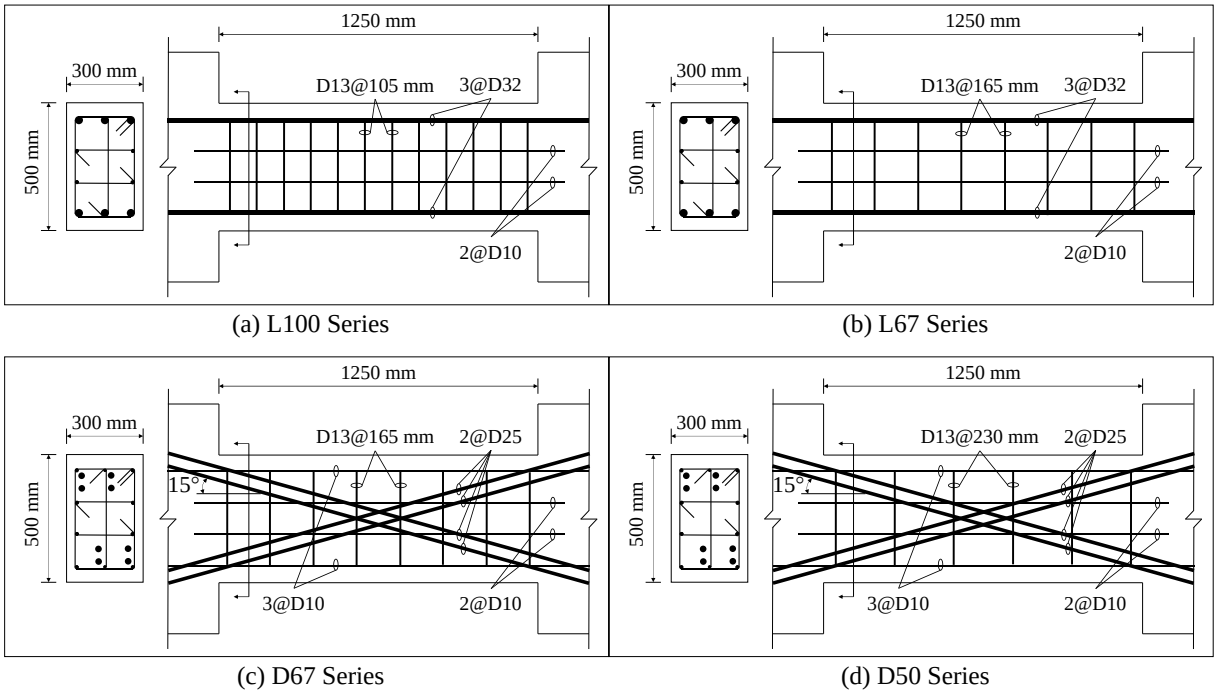

Figure 1 Specimen layout

Material properties

A normal-weight concrete with a design 28-day concrete compressive strength (f'_c) of 30 MPa (4.4 ksi) was specified for all specimens. The maximum aggregate size of 25 mm (1 in.) and a slump of 150 mm (5.9 in.) were requested. Concrete strength was determined based on the average of three standard 100 mm × 200 mm (4 in. × 8 in.) cylinders for each series. All cylinders were cast on the same day along with casting specimens from each concrete truck at a local concrete plant. Korean Standard (KS) SD400 deformed bars with a nominal yield strength (f_y) of 400 MPa (58 ksi) were specified for steel rebars. The average yield strength and ultimate strength (f_u) for each size were determined by performing direct tensile tests on three 500 mm(19.7 in.)-long specimens. Test results of concrete and steel rebars are shown in Table 1.

Table 1 Measured material properties

Series	Concrete f'_c, MPa	Steel reinforcement, MPa							
		D32		D25		D13		D10	
		f_y	f_u	f_y	f_u	f_y	f_u	f_y	f_u
L100	32.2	461.7	645.1	-	-	465.3	702.3	433.7	685.6
L67	32.5								
D67	32.2	-	-	427.6	668.6				
D50	28.9								

Test setup

Coupling beams experience both a prominent lateral displacement and a slight axial compressive deformation when a building has a large deformation as shown in **Figure 2**. To imitate this mechanism, RC coupling beams were positioned vertically and embedded between two adjacent stiff RC blocks, and the top blocks were fixed to the upper steel frame which was connected to a hydraulic actuator and two steel links with four pin connections. The bottom block was enlarged for avoiding overturning and bolted to the laboratory's strong floor. The test setup is illustrated in **Figure 3**.

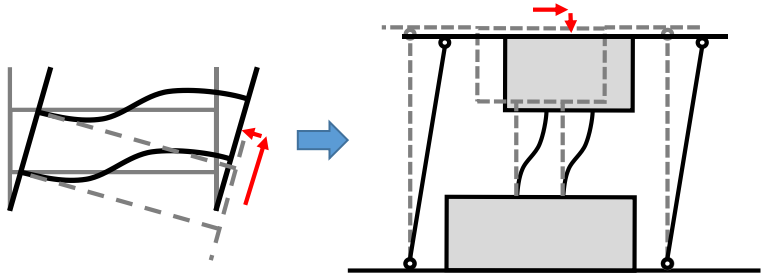

Figure 2 Oscillating mechanism

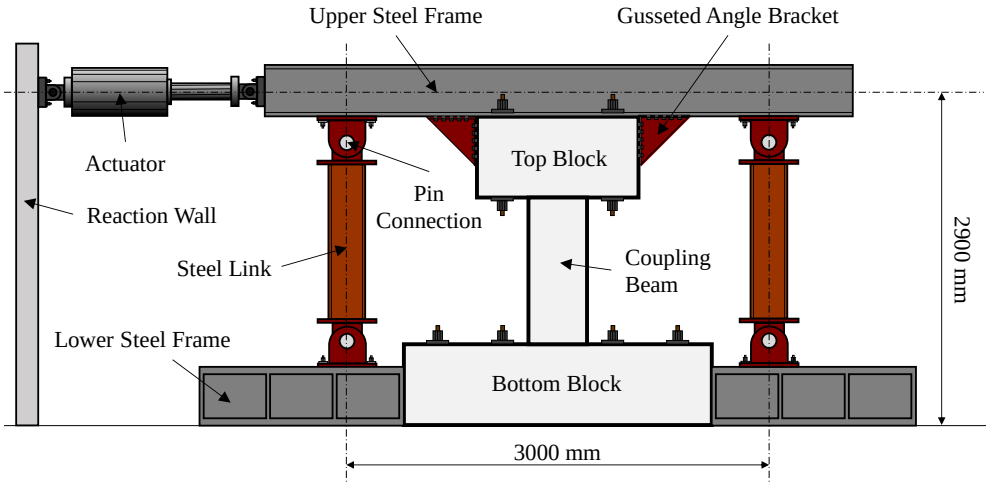

Figure 3 Test setup

Loading protocols

In this study, the actuator was displacement-controlled to apply both seismic load and wind load to each series. **Figure 4** shows the seismic loading protocol with two cycles at each stage, which was recommended by ACI 374.2R-13. The simulated wind load was developed with a zero-mean process based on 35- to 70-story buildings (150- to 300-meter heights, the typical height of Korea's 300 tallest buildings). The prescribed maximum ductility demand was set as $1.5\theta_y$ to reach the inelastic behavior, which corresponds to the wind load reduction factor (R_{WR}) of 1.4 based on the equal energy principle (**Figure 5**), where the yield drift ratio (θ_y) is designated by the result of specimen tested under seismic load. The number of cycles in each stage with the same increasing increments of $0.25\theta_y$ was defined by the Gaussian distribution of the peak factor (g_L) in the across-wind direction in KBC 2016 (2016) as shown in **Figure 6** and **Table 2**. Finally, the wind load can be composed of 900 linear cycles and 15 non-linear cycles as shown in **Figure 7**.

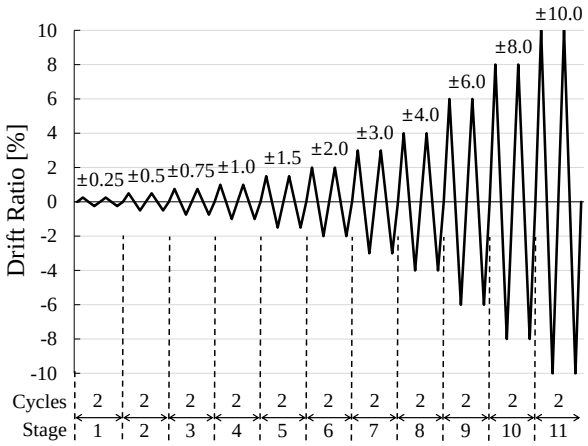

Figure 4 Seismic loading protocol

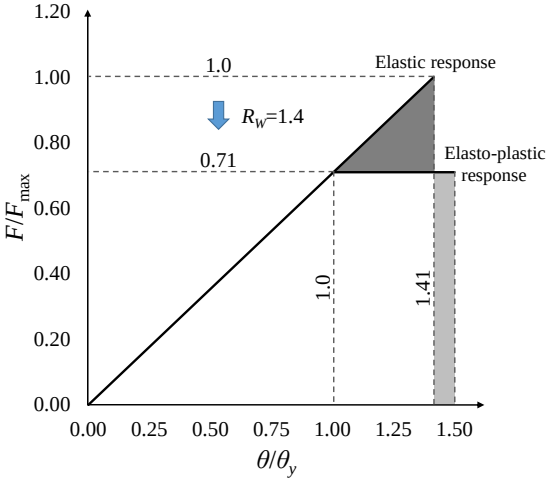

Figure 5 Equal energy principle

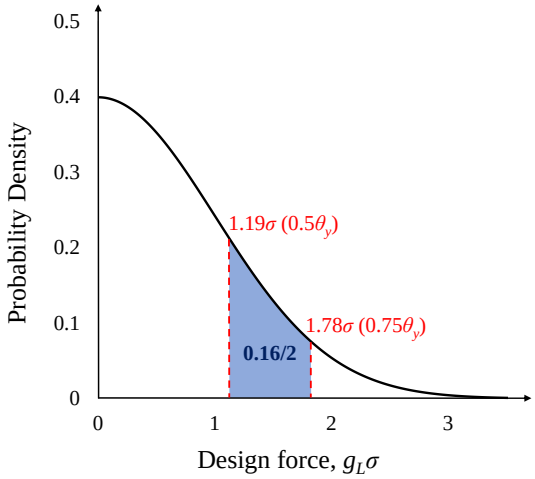

Figure 6 Gaussian distribution (based on a 200-meter-height building)

Table 2 Cycle configuration

Design displacement	Force ratio (F/F_{max})	Design force	Probability	Expected No. of cycles	Design No. of cycles
$1.5\theta_y$	1.00	$3.23\sigma \sim 3.44\sigma (= g_L\sigma)$	0.002 ~ 0.004	2 ~ 3	3
$1.25\theta_y$	0.87	$2.80\sigma \sim 2.98\sigma$	0.012 ~ 0.017	11 ~ 15	12
$1.0\theta_y$	0.71	$2.28\sigma \sim 2.43\sigma$	0.054 ~ 0.065	39 ~ 65	50
$0.75\theta_y$	0.53	$1.71\sigma \sim 1.82\sigma$	0.158 ~ 0.167	101 ~ 191	150
$0.5\theta_y$	0.35	$1.14\sigma \sim 1.22\sigma$	0.314 ~ 0.322	191 ~ 391	300
$0.25\theta_y$	0.18	$0.57\sigma \sim 0.61\sigma$	0.431 ~ 0.451	261 ~ 547	400

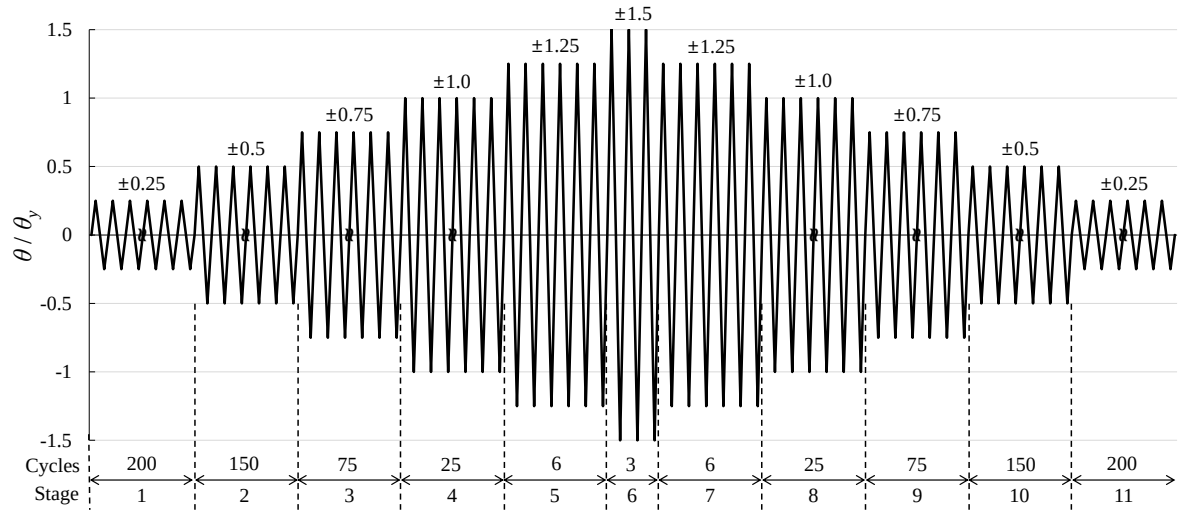

Figure 7 Wind loading protocol

TEST RESULTS

Hysteretic behaviors

In this study, both seismic and wind loads were applied to four series of eight RC coupling beams. Each specimen tested under wind load took more than 10 hours, whereas those tested under seismic load needed only 4 hours. Test results are shown in **Figure 8**. For specimens tested under seismic load (named "Series-S"), specimen L100-S exhibited its peak shear strength (V_{test}) of 684.2 kN (153.8 kips), but the test was subsequently stopped due to the occurrence of unexpected out-of-plane displacement. Specimen L67-S had a lower peak shear strength of 632.1 kN (142.1 kips) than L100-S, because the number of transverse reinforcements was reduced from 11 for L100-S to 8 for L67-S. Because diagonal reinforcements can function as flexural and shear reinforcements simultaneously, specimen D67-W presented well-rounded hysteretic loops with a larger peak shear strength of 809.0 kN (181.9 kips) than L67-S. After the number of transverse reinforcements was reduced from 67% to 50%, specimen D50-S had lower peak shear strength of -761.4 kN (171.2 kips).

This study reconfirmed that DRCCBs had superior shear strength, ductility, and energy dissipation than LRCCBs due to the lack of pinching effect. However, as can be seen in **Figure 8**, the shear strengths of DRCCBs were notably larger than the nominal shear strength (V_n) and the upper limit ($V_{n,upper}$, which equals $0.83\sqrt{f'_c}A_{cw}$) in ACI 318-19, and this underestimation may incur unexpected force or damage at the web or adjacent walls. Additionally, since transverse reinforcements had an influence on shear strength, considering the contribution of transverse reinforcement is recommended in DRCCBs' design procedure. Overall, the test results of hysteretic behavior signal that DRCCBs with half of the required transverse reinforcements and LRCCBs with two-thirds of the requirement are likely to be applied to the case of low-to-moderate seismicity and high wind hazard.

With regard to specimens subjected to wind load (named "Series-W"), all specimens presented more pinching effect after Stage 6 as shown in **Figure 9**, but there was no occurrence of extensive damage and only minor cracks with widths ranging from 0.35 to 2.0 mm (0.014 to 0.079 in.) were observed, which can be categorized into "Insignificant Damage" in FEMA 306. Therefore, the tests performed in this study can be seen as an example of the application of the performance-based wind design framework.

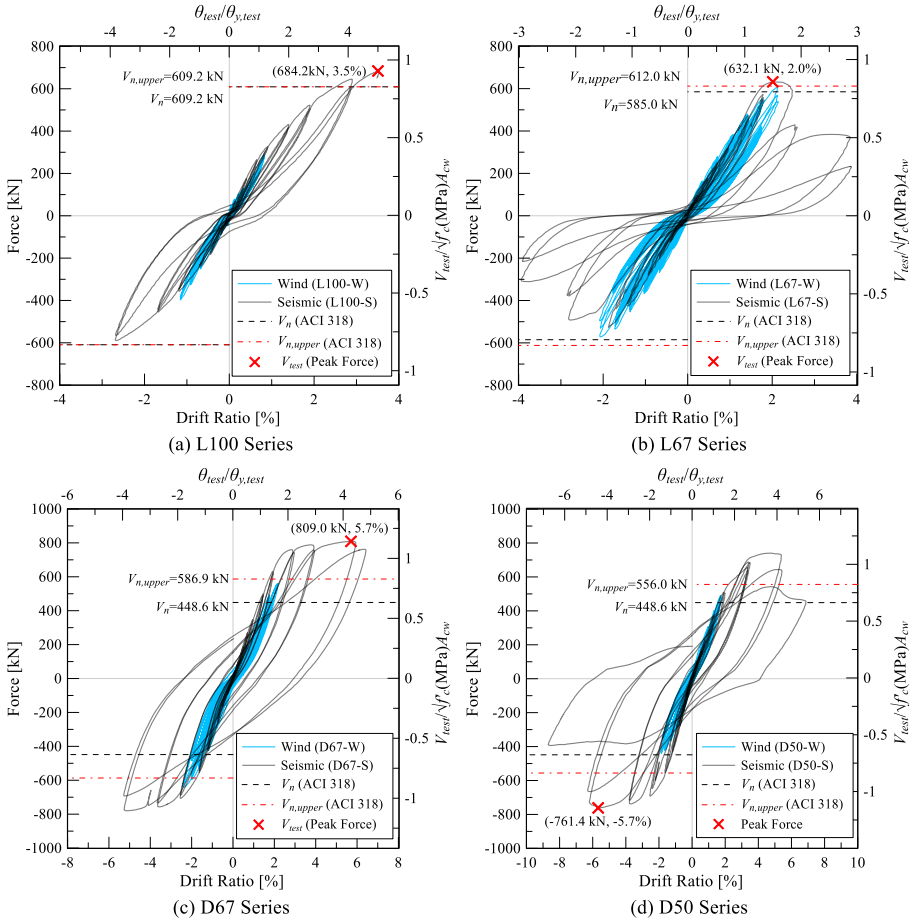

(a) L100 Series (b) L67 Series

(c) D67 Series (d) D50 Series

Figure 8 Load-rotation curves

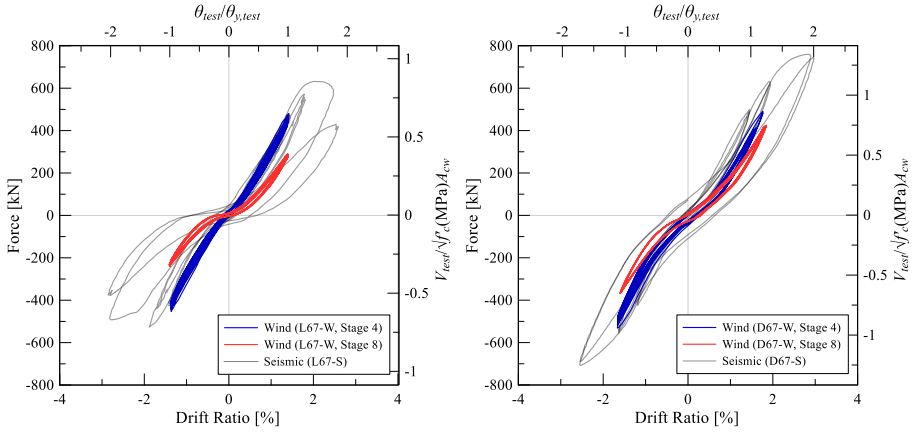

(a) L67 Series (b) D67 Series

Figure 9 Load-rotation curves at $1.0\theta_y$

Drift contribution

The contribution of four components to the overall chord rotation, including shear deformation of the beam, flexure or curvature deformation of the beam, bar slip or extension at the beam ends, and sliding at the beam ends, were examined to better understand how the RC coupling beams behaved during the test. The results, shown in **Figure 10**, demonstrate that the initial overall chord rotation for all specimens was mostly caused by shear and flexure deformation. Shear deformation had the largest percentage increase among the four components, which accounted for more than 70% and 60% for seismic and wind load in the final stage, respectively; in contrast, the proportion of flexure deformation sharply decreased to just 10% in the final stage. This is due to the fact that when deformation demand increased, inclined shear cracks formed more quickly than flexural cracks, finally leading to failure. While the contribution of bar slip/extension had some fluctuations with an approximate value of 25%, sliding showed a steady contribution at less than 10% for all test specimens.

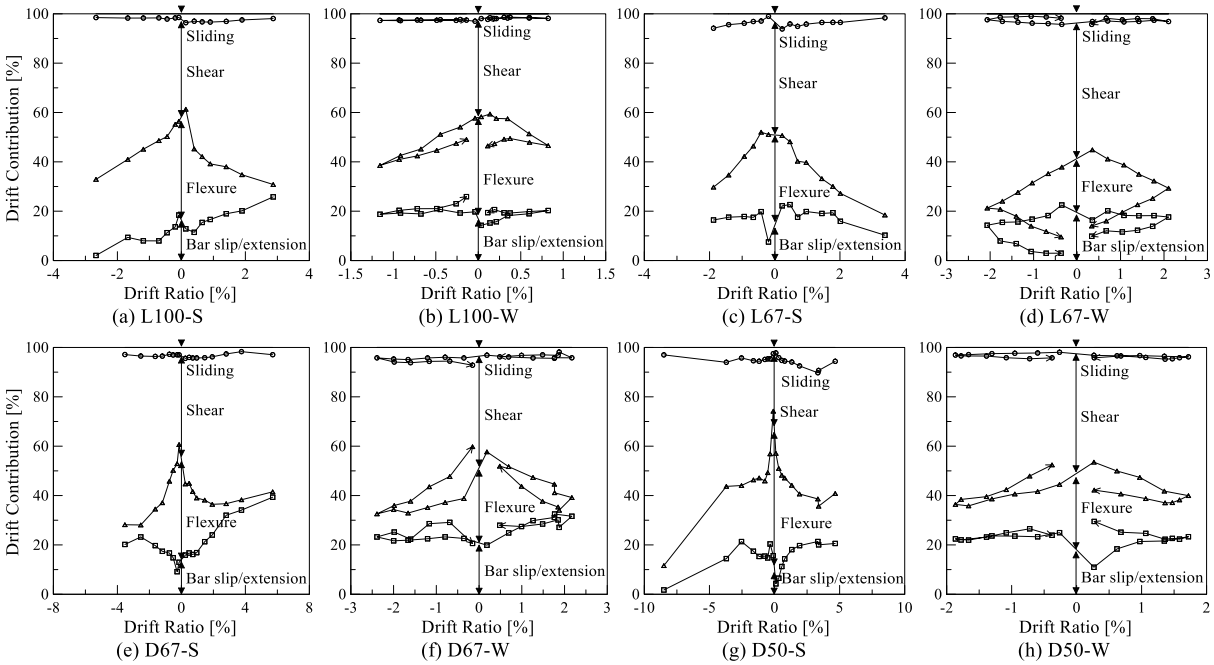

Figure 10 Drift contribution

Stiffness

The effective flexural stiffness (E_cI_{eff}) and effective shear stiffness (G_cA_{eff}) of the specimens were estimated, which was defined as $K_f \times l_n^3/12$ and $K_s \times l_n$, respectively, where the K_f and K_s were $0.6V_{y,test}$ divided by flexural deformation and shear deformation respectively, $V_{y,test}$ was obtained when a main (longitudinal or diagonal) reinforcement first reached yield strain during the test, the flexural deformation including flexure and bar slip/extension was taken as the deformation ($\Delta_{0.6V_{y,test}}$) times the percentage of the two components, and shear deformation was taken as the corresponding deformation times the percentage of shear and sliding components from drift contribution. As can be seen in **Figure 11**, test results of effective flexural stiffness values (E_cI_{eff}/E_cI_g) ranging from 0.09 to 0.14 are closer to the value suggested by PEER/ATC 72-1 and effective shear stiffness values (G_cA_{eff}/G_cA_g) between about 0.04 and 0.05 are significantly less than the values proposed in TBI 2017 (2017) and PEER/ATC 72-1 (2010)., where I_g is the moment of inertia and area, and A_g is the gross concrete section.

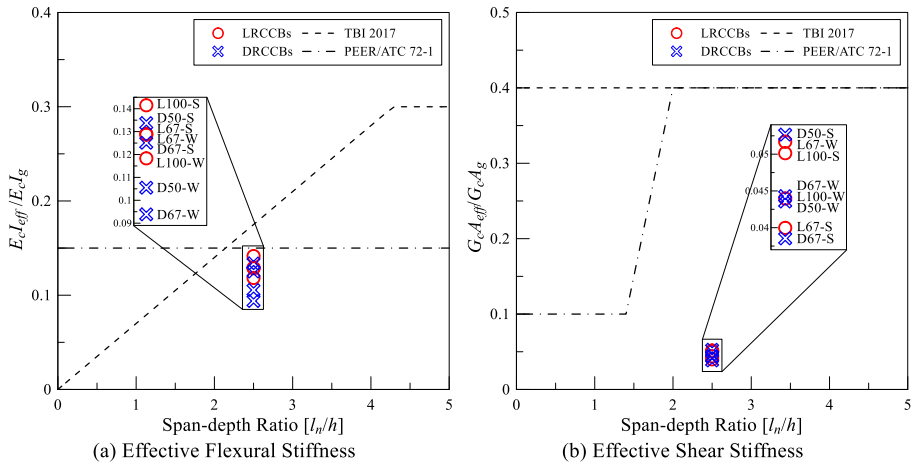

Figure 11 Effective stiffness

The secant stiffness (E_cI_{sec}), which was defined as the ratio of the shear strength to the maximum displacement, is shown in **Figure 12** as the secant stiffness at each stage divided by the initial secant stiffness ($[E_cI_{sec}]_{initial}$). The secant stiffness for specimens subjected to seismic load rapidly decreased after Stage 4 due to increased displacement requirements. For specimens tested under the wind load, the high number of testing cycles resulted

in a dramatic decline at Stage 2, but their values of $E_cI_{sec}/(E_cI_{sec})_{initial}$ showed a steady decline after Stage 4. However, since pinching behavior becomes more conspicuous due to cyclic softening despite specimens having smaller displacement demands after yielding, low-cycle fatigue failure may occur under an extremely large number of cycles, but the effect of low-cycle fatigue needs more investigation.

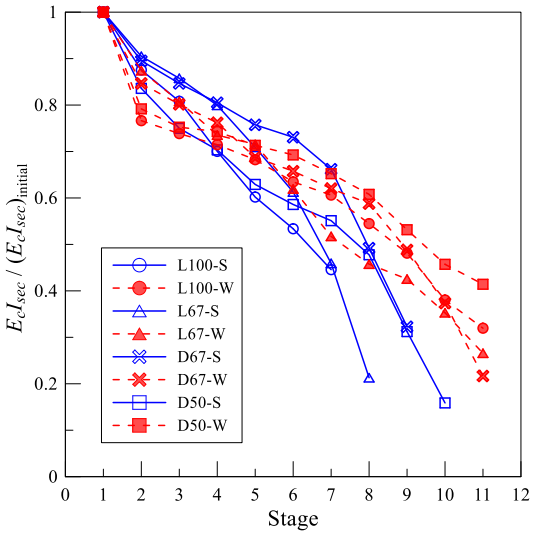

Figure 12 Secant stiffness

CONCLUSION

In this study, the following conclusions and recommendations are drawn based on the cyclic seismic and wind loading tests of eight RC coupling beams with a span depth ratio (l_n/h) of 2.5 and four different layouts.

1. DRCCBs had superiority of shear strength, ductility and energy dissipation due to the lack of pinching effects. Improvement of the nominal shear strength and upper limit in ACI 318-19 is suggested for DRCCBs, because the underestimation of their shear strength may result in undesirable forces or damage to the coupled wall system. Taking transverse reinforcements into account for better shear strength prediction is also advised, which is likely to implement a more efficient and economical design for areas with low-to-moderate seismicity and high wind.

2. The tests subjected to the simulated wind event with R_{WR} of 1.4 can be deemed an experimental example of applying performance-based wind design, which can be classified as "Insignificant Damage" in FEMA 306. Nevertheless, due to the symptom of cyclic softening, the effect of low-cycle fatigue requires more investigation.

REFERENCES

ACI Committee 318 (2019), "Building Code Requirements for Structural Concrete (ACI 318-19) and Commentary (ACI 318R-19)," American Concrete Institute, Farmington Hills, MI.

ACI Committee 374 (2013), "Guide for Testing Reinforced Concrete Structural Elements under Slowly Applied Simulated Seismic Loads (ACI 374.2R-13)," American Concrete Institute, Farmington Hills, MI.

Abdullah, S. A.; Aswegan, K.; Klemencic, R.; and Wallace, J. W. (2020), "Performance of Reinforced Concrete Coupling Beams Subjected to Simulated Wind Loading," *ACI Structural Journal*, Vol. 117, No.3, 283-295.

Alinejad, H.; and Kang, T. H.-K. (2020), "Engineering Review of ASCE 7-16 Wind-Load Provisions and Wind Effect on Tall Concrete-Frame Buildings," *Journal of Structural Engineering*, Vol. 146, No. 6, 04020089.

ASCE (2019), "Prestandard for Performance-Based Wind Design," American Society of Civil Engineers, Reston, VA.

ASCE (2022), "Minimum Design Loads and Associated Criteria for Buildings and Other Structures (ASCE 7-22)," American Society of Civil Engineers, Reston, VA.

Aswegan, K.; Larsen, R.; Klemencic, R.; Hooper, J.; and Hasselbauer, J. (2017), “Performance-Based Wind and Seismic Engineering: Benefits and Considering Multiple Hazards,” *Structures Congress 2017*, 473-484.

Cheng, M.-Y.; Gitomarsono, J.; and Zeng, H.-Y. (2019), "Cyclic Test of Diagonally Reinforced Concrete Coupling Beam with Different Shear Demand," *ACI Structural Journal*, Vol. 116, No. 6, 241-250.

Han, S. W.; Kim S. B.; and Kim T. (2019), “Effect of transverse reinforcement on the seismic behavior of diagonally reinforced concrete coupling beams,” *Engineering Structure*, Vol. 196, 109307.

Jeong, S. Y.; Alinejad, H.; and Kang, T. H.-K. (2021), “Performance-Based Wind Design of High-Rise Buildings Using Generated Time-History Wind Loads,” *Journal of Structural Engineering*, Vol. 147, No. 9, 04021134.

KBC (2016), “Korean Building Code (KBC 2016)”, Ministry of Land, Infrastructure and Transport of Korea, Seoul, Korea. (in Korean)

Lim, E.; Hwang, S.-J.; Wang, T.-W; and Chang, Y.-H. (2016a), “An investigation on the seismic behavior of deep reinforced concrete coupling beams,” *ACI Structural Journal*, Vol. 113, No. 2, 1-10.

Lim, E.; Hwang, S.-J.; Cheng, C.-H; and Lin, P.-Y. (2016b), “Cycling tests of reinforced concrete coupling beams with intermediate span-depth ratio,” *ACI Structural Journal*, Vol. 113, No. 3, 515-524.

Naish, D.; Fry, A.; Klemencic, R.; and Wallace, J. (2013), “Reinforced Concrete Coupling Beams. Part I: Testing,” *ACI Structural Journal*, Vol. 110, No. 6, 1057-1066.